Dalton Transactions

Reversible Modulation of the Redox Characteristics of Acid-Sensitive Molybdenum and Tungsten Scropionate Complexes

Journal:	*Dalton Transactions*
Manuscript ID	DT-ART-02-2018-000598.R1
Article Type:	Paper
Date Submitted by the Author:	20-Mar-2018
Complete List of Authors:	Heyer, Alexander; University of Virginia, Department of Chemistry Shivokevich, Philip; University of Virginia, Department of Chemistry Hooe, Shelby; University of Virginia, Department of Chemistry Welch, Kevin; University of Virginia, Department of Chemistry Harman, W.; University of Virginia, Department of Chemistry Machan, Charles; University of Virginia, Department of Chemistry

Journal Name

ARTICLE

Reversible Modulation of the Redox Characteristics of Acid-Sensitive Molybdenum and Tungsten Scorpionate Complexes

Received 00th January 20xx,
Accepted 00th January 20xx

DOI: 10.1039/x0xx00000x

www.rsc.org/

Alexander J. Heyer,† Philip J. Shivokevich,† Shelby L. Hooe, Kevin D. Welch, W. Dean Harman,* and Charles W. Machan*

The large-scale synthesis of the scorpionate ligand Ttz (hydrotris(1,2,4-triazol-1-yl)borate) is reported as well as syntheses of Group VI complexes K[M(L)(CO)$_3$] and M(L)(NO)(CO)$_2$ (L = Ttz or Tp (hydrotris(pyrazol-1-yl)borate), M = Mo or W). The redox characteristics of the metal in these Ttz complexes are shown to be reversibly modulated by interactions between the exo-4-N lone pairs of the triazolyl rings and Brønsted or Lewis acids. The basicity of the scorpionate ligand in [M(Ttz)(CO)$_3$]$^-$ is quantified (pK_a^{H2O} values range from 1.1 to 4.6) and found to be dependent on both the oxidation state and identity of metal. In the presence of Brønsted acids, the observed redox behavior for the one-electron oxidation of the Group VI metal center is consistent with a proton-coupled electron transfer (PCET). Indeed, for both Mo and W derivatives, a one-electron oxidation decreases the pK_a by ~3.5 units.

Introduction

Since their introduction in 1966,[1] scorpionate ligands have enjoyed widespread popularity in applications ranging from catalysis to enzyme active-site modeling. The bulk of research done with these versatile ligands has been with the pyrazole analogue, hydrotris(pyrazol-1-yl)borate (Tp), and derivatives made from substituted pyrazoles (Figure 1).[1-7] Despite being introduced by Trofimenko along with Tp in his original reports[3], hydrotris(1,2,4-triazol-1-yl)borate (Ttz), was largely ignored for two decades until a detailed synthesis for the free ligand was reported by Lobbia and co-workers.[8] Since then, dozens of reports have appeared describing transition metal complexes with Ttz[9-14] and alkylated analogues.[15-21] The additional nitrogen in this triazole-based scorpionate causes the ligand to be less electron-donating, but more water-soluble than the more ubiquitous pyrazole cousin (**Figure 1**).

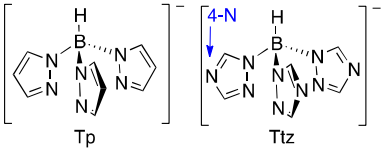

Figure 1. Structure of scorpionate ligands [Tp]$^-$ and [Ttz]$^-$.

Significantly, several recent studies have explored the modulation of the σ-donor properties of Ttz via chemical interactions of the exo-nitrogen (4-N). Pioneering work by Papish and co-workers found that ligand protonation of Ttz complexes of first-row metals can have a significant effect on the electron density at the metal center,[15-18,21-23] and that these properties can be used to influence catalytic behavior.[22, 24, 25] Based on these prior results, we were interested in quantifying the effects of metal oxidation state on the ability of the Ttz ligand to interact with exogenous acids (**Figure 2**).

Herein we report the electrochemical modulation of the basicity of the exo-N atoms of the Ttz ligand based on the oxidation state of the Group VI metal centers. Titration studies and thermochemical cycles have enabled direct quantification of the pK_a of the protonated exo-4-N atoms for the M(0) oxidation state, and the subsequent decrease in pK_a of ~3.5 upon oxidation to the M(I) state, for both Mo and W. Interestingly, these redox-induced acidity changes behave as proton-coupled electron transfer (PCET) reactions in cyclic voltammetry (CV) experiments.

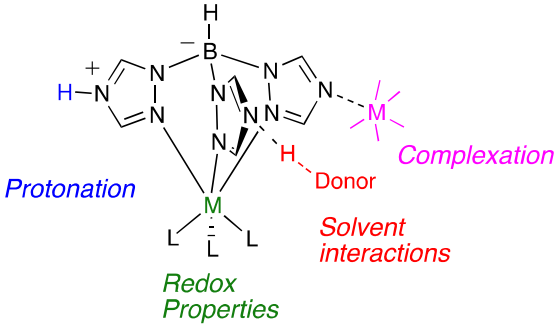

[a] Department of Chemistry, University of Virginia, McCormick Road, P.O. Box 400319, Charlottesville, VA 22904-4319.
† These authors contributed equally
* wdh5z@virginia.edu, 0000-0003-0939-6980; machan@virginia.edu, 0000-0002-5182-1138
Electronic Supplementary Information (ESI) available: description of NMR-based pK_a determination, additional CVs, coordinates and plots from DFT calculations, additional IR-SEC spectra. See DOI: 10.1039/x0xx00000x

Figure 2. Possible chemical interactions with d^6 metal complexes using the Ttz ligand framework that could alter the metal-based redox potentials.

Results and Discussion

Synthetic Procedures

Using a modified literature procedure,[3, 8] K[Ttz] (**1**) was isolated by bringing a mixture of 1,2,4-triazole and KBH_4 to a molten flux at 190 °C until H_2 evolution ceased. The resulting solid was purified under vacuum with heating to remove excess triazole. Ligand **1** was then recrystallized from acetone. This procedure obtains reproducible results on a >100 g scale (up to 168 g, ~2/3 mole K[Ttz] isolated) with a consistent >80% yield (based on KBH_4) and high purity (**See Experimental Section**).

With large quantities of K[Ttz] in hand, eight model complexes were subsequently isolated to compare the Tp^- and Ttz^- ligands: $[M(Tp)(CO)_3]^-$ (M = Mo (**2**$^-$), W (**4**$^-$)), $[M(Ttz)(CO)_3]^-$ (M = Mo (**3**$^-$), W (**5**$^-$)), $M(Tp)(NO)(CO)_2$ (M = Mo (**6**), W (**8**)), and $M(Ttz)(NO)(CO)_2$ (M = Mo (**7**) or W (**9**)). The Tp complexes **2**$^-$, **4**$^-$, **6**, and **8** were first reported by Trofimenko, McCleverty and co-workers,[5,6,26] and the Ttz analogues follow a similar synthetic procedure,[11] with the exception of complexes **7** and **9**, which were produced using the nitrosylation process reported by Dilsky and co-workers (**Scheme 1**).[27] All analyses of anionic species were performed with potassium as the counterion except for those of **5**$^-$ in acetonitrile, where the potassium was exchanged for tetraethylammonium to improve solubility.

Scheme 1. Synthesis of molybdenum and tungsten nitrosyl complexes of the scorpionate ligand Ttz.

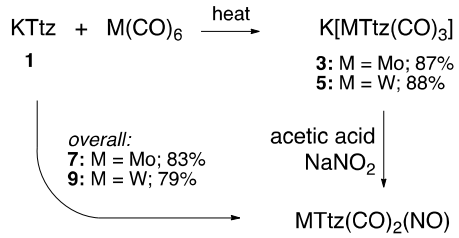

Table 1 compares the M(I)/(0) reduction potentials (E^0 vs NHE) and carbonyl and nitrosyl IR absorption bands (wavenumbers, cm^{-1}) of the complexes **2**-**9**. Replacing Tp with Ttz results in an increase of the observed CO stretching frequencies by 10-20 cm^{-1}, similar to the shift reported by Papish and co-workers for $Cu(Ttz^{tBu,Me})(CO)$ in comparison to the Tp analogue.[21] A similar shift occurs for the nitrosyl stretch of **6** and **7**, where the observed IR absorption band for $Mo(Ttz)(CO)_2(NO)$ (**7**) at 1654 cm^{-1} is significantly higher in energy than what we recorded for the Tp analogue (**6**) (1642 cm^{-1}; *Nota bene*: this value differs from a previously reported value for **6** recorded under different conditions).[11] Significantly, the M(I)/(0) reduction potentials of the d^6 Ttz complexes are 0.15 – 0.25 V more positive than the comparable Tp derivatives, consistent with a more electron-deficient metal center in the Ttz systems. These findings are in agreement with calculations performed by Lu and co-workers.[28] To simplify subsequent analyses, we focused on the tricarbonyl derivatives to limit the scope of possible IR-active isomers in solution and because of the chemical irreversibility in the I/0 couple for the nitrosyl derivatives.

Table 1. Comparison of CV and IR data for Mo and W complexes with Tp and Ttz.

Complex	ν_{CO} (cm^{-1})[a]	ν_{NO} (cm^{-1})[a]	$E_{(I/0)}$ (V)[b]
$[Mo(Tp)(CO)_3]^-$ (**2**$^-$)	1761, 1894	-	0.02*
$[Mo(Ttz)(CO)_3]^-$ (**3**$^-$)	1773, 1905	-	0.22*
$[W(Tp)(CO)_3]^-$ (**4**$^-$)	1750, 1882	-	-0.07*
$[W(Ttz)(CO)_3]^-$ (**5**$^-$)	1772, 1905	-	0.17*
$Mo(Tp)(CO)_2(NO)$ (**6**)	1898, 2001	1642	1.18†
$Mo(Ttz)(CO)_2(NO)$ (**7**)	1910, 2010	1654	1.30†
$W(Tp)(CO)_2(NO)$ (**8**)	1874, 1986	1624	1.12†
$W(Ttz)(CO)_2(NO)$ (**9**)	1884, 1994	1636	1.26†
3$^-$ + DPhAT[c]	1791, 1918	-	0.43*
5$^-$ + DPhAT[c]	1791, 1918	-	0.38*
3$^-$ + BF_3•Et_2O[c]	1787, 1920	-	0.43*
3$^-$ + $Sc(OTf)_3$[c]	1792, 1919	-	0.51*
5$^-$ + BF_3•Et_2O[c]	1788, 1911	-	0.39*

a IR spectra recorded from glaze on salt plate *b*. CV recorded at 100 mV/s in acetonitrile solution with TBAH electrolyte (NHE). * indicates $E_{½}$ † indicates $E_{p,a}$ c. 0.00003 M acid to 0.00001 M **3** and **5**. In-situ for CV, glaze for IR

Chemical Acid-Base Modulation

Previously, Papish and co-workers demonstrated that the $Ttz^{tBu,Me}$ ligand in the complex $Cu(Ttz^{tBu,Me})(CO)$ could be protonated at an exo nitrogen (4-N) using one equivalent of HBF_4.[21,22] Solution IR data obtained in CH_2Cl_2 indicated that two equivalents of acid resulted in an additional protonation, and the assignment of the observed vibrational frequencies were corroborated by DFT calculations. The authors also confirmed the reversibility of the protonation reaction by adding an appropriate amine base, whereupon the exo nitrogen was deprotonated.[21,22] Titration of HBF_4 in a CH_3CN/H_2O solvent mixture with $Cu(Ttz^{tBu,Me})(CO)$ suggested that that the first and second protonation of the ligand framework happen at similar pH such that $pK_a(1) \sim pK_a(2) \sim 3.5$.

In our initial experiments, when complexes **3**$^-$ or **5**$^-$ were added to an acetonitrile solution of diphenylammonium triflate (DPhAT $pK_a^{AN} = 5.97$) and dropcast onto a salt plate, a ~ +20 cm^{-1} ν_{CO} shift from the starting material was observed (**Table 1**), analogous to carbonyl IR absorption band shifts reported for a single protonation of the $Cu(Ttz^{tBu,Me})(CO)$ system.[21,22] Interestingly, the protonation reaction also caused a shift in the M(I)/(0) reduction to more positive potentials by 200 mV according to CV data (**Figure 3**). We assign these new redox features to a monoprotonated product of the starting materials: $Mo(HTtz)(CO)_3$ **3H** and $W(HTtz)(CO)_3$ **5H**, respectively.

Remarkably, exposure to stronger acids, e.g. triflic acid (pk_a^{AN} = 0.7),[29,30] showed *no further change* in the cyclic voltammogram (up to 0.1 M HOTf (10 eq)) beyond the single protonation product. This observation is in contrast to the

double-protonation observed by Papish and co-workers.[18] Protonation of **3** and **5** was reversible upon addition of the base triethylamine (TEA) (**Figure 3**).

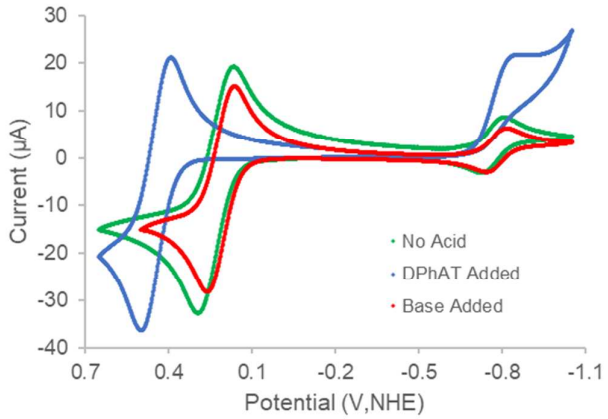

Figure 3. Cyclic voltammogram of reversible acid addition to $MoTtz(CO)_3$. Base: triethylamine; acid: DPhATt; 10 equivalent portions with respect to **3**$^-$. Colbatocenium hexafluorophosphate was used as internal standard, $E_{1/2}$ = -0.78 V vs NHE. The irreversibility of the cobaltocene redox wave in the presence of acid is attributed to a chemical reaction under these conditions; control experiments in the absence of **3**$^-$ show an identical response with added acid.[51]

To quantify the basicity of the exo nitrogen, the pK_a^{AN} and pK_a^{DMSO} were determined for **3H** and **5H** using the method of equilibration with an acid of known pK_a^{AN} and pK_a^{DMSO} (pyridinium triflate: pK_a^{AN} = 12.53 and pK_a^{DMSO} = 3.4).[31-33] In DMSO, the conjugate acid of the Mo and W analogues were both found to have a pK_a^{DMSO} of 1.8.[32,33] Shifting to the more acidic solvent system MeCN, pK_a^{AN} values were determined to be 11.0 for **3H** and 11.9 for **5H** (also using pyridinium triflate; pK_a^{AN} = 12.53). Converting these values to an aqueous scale by the method of Leito and co-workers,[33] where pK_a^{AN} = 6.04 + 1.269(pK_a^{H2O}), we find that complexes **3**$^-$ (3.9) and **5**$^-$ (4.6) are notably more basic than $CuTtz^{tBu,Me}(CO)$ (3.5), despite the latter system having alkyl substituents on the triazole rings.[21-23]

The ^{1}H NMR spectrum obtained for **5**$^-$ in the presence of weaker acids than DPhAT exhibits two pairs of broadened triazolyl resonances in an approximately 2:1 ratio, consistent with the anticipated reduced symmetry of a monoprotonated complex such as $W(HTtz)(CO)_3$ **5H**. The monoprotonation of **5**$^-$ is observed using either pyridinium triflate or (p-methoxyanilinium)[BF_4] (pK_a^{AN} = 11.86) as the acid source. Equilibration with either acid gives a pK_a^{AN} for **5H** of 11.9. Similar results are obtained for related experiments using **3**$^-$; however, the broadening of **5**$^-$ on the NMR timescale is suggestive of a slower rate of proton exchange than that for **3**$^-$, which shows a sharp pair of averaged Ttz resonances under analogous conditions.

With the reduction potentials for both protonated and deprotonated complexes (**3**$^-$, **3H**, **5**$^-$, **5H**) and pK_a values for the conjugate acids (**3H**, **5H**) in hand, a thermodynamic cycle could be constructed to determine the pK_a for their oxidized forms, $[Mo^I(HTtz)(CO)_3]^+$ **3H**$^+$ and $[W^I(HTtz)(CO)_3]^+$ **5H**$^+$. An example of this calculation is provided in **Figure 4** for the Mo analogue (**3**$^-$), where the pK_a of **3H**$^+$ is estimated to be 7.5 (See **Supporting Information**). By an analogous process, the complex **5H**$^+$ was determined to have a pK_a^{AN} of 8.4. These results are summarized in **Table 2**. Notably, a ΔpK_a^{AN} of 3.5 is obtained for both Group VI congeners upon one-electron oxidation, pointing to a similar electronic influence of the metal centers on the basicity of the ligand.

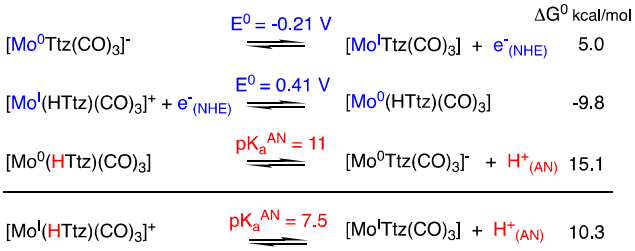

Figure 4. Determination of pK_a^{AN} of $[Mo(HTtz)(CO)_3]^+$ (**3H**$^+$).

Table 2. pK_a values for several Ttz complexes.

Complex	pK_a^{AN}	pK_a^{H2O}
$[Mo^0(HTtz)(CO)_3]$	11	3.9
$[Mo^I(HTtz)(CO)_3]^+$	7.5	1.1
$[W^0(HTtz)(CO)_3]$	11.9	4.6
$[W^I(HTtz)(CO)_3]^+$	8.4	1.8
$[Cu^I(HTtz^{tBu,Me})(CO)]^+$	10.5	3.5

Electrochemical Control of Acidity

The large difference in pK_a values between the neutral and oxidized species in **Table 2** indicates that with low concentrations of weaker acids, the anionic starting materials are protonated, but their corresponding oxidized forms are not. To further understand the difference in basicity of the Ttz ligand in **3**$^-$ and **5**$^-$ compared to $Cu(Ttz^{tBu,Me})(CO)$, the effects of metal-based oxidations on the acidity of the protonated ligand framework were also investigated by CV through titration studies. Indeed, titration experiments with weaker acids exhibit the characteristics of concentration-dependent reduction potential for the half reaction by CV:

$$[M^ITtz(CO)_3] + H^+ + e^- \rightarrow [M^0(HTtz)(CO)_3] \quad (1)$$

Using a procedure described by Dempsey and co-workers for the examination of proton-coupled electron transfer (PCET) reactions in non-aqueous systems,[34] a solution of complex **3**$^-$ was examined across a $\log_{10}([A]/[HA^+])$ range of -1.0 to 0.4 using 2-methoxypyridinium triflate (HA^+) and 2-methoxypyridine (A). The resulting I/0 potentials, as determined CV, were plotted against the $\log_{10}([A]/[HA^+])$ to generate the Nernstian plot shown in **Figure 5**. The given slope of 55 mV/decade suggests a single proton transfer reaction per electron, which is indicative of PCET. Repeating this

experiment for the W analogue **5**$^-$, from $\log_{10}([A]/[HA^+])$ = -0.15 to 0.45 (**Figure 5**, bottom), generated a slope of 66 mV/decade, consistent with a single proton donor-acceptor interaction for every electron transferred.

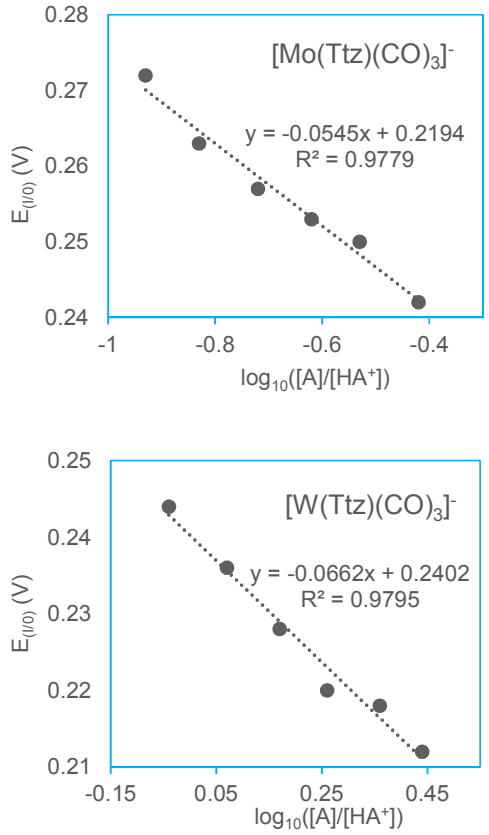

Figure 5. Nernst plots for **3**$^-$ (top) and **5**$^-$ (bottom).

To validate the mechanistic assignments for the one-electron oxidized species **3**, **3H**$^+$, **5**, and **5H**$^+$ obtained using different acids, electrochemical speciation was examined through IR-SEC. IR-SEC enables changes in an analyte of interest to be monitored as a function of potential and time.[35] Using this technique, CV data can be directly correlated to spectra detailing molecular composition. A customized electrochemical cell was charged with an acetonitrile solution of either **3**$^-$ or **5**$^-$ with TBAH electrolyte. IR spectra were recorded at a series of potentials to monitor transformations at the electrode surface (see Supporting Information).[35]

At resting potential without added acid, two intense bands assigned to carbonyl modes are observed at 1905 and 1774 cm^{-1} for **3**$^-$ (**Figure 6; Table 3**). DFT calculations suggest that the band at 1906 cm^{-1} corresponds to a single symmetric stretching mode, whereas the broad and more intense band at 1774 cm^{-1} is a combination of two asymmetric stretching modes, *vide infra*. Generally, the carbonyl IR modes calculated by DFT are in qualitative agreement with the experimental values (**Table 4**). If the cell potential is increased stepwise towards 0.8 V vs NHE, where the proposed one-electron oxidation is observed by CV, these bands diminish in intensity with the concomitant appearance of new absorbance bands. The most intense bands are centered around 2021 and 1894 cm^{-1}. A similar shift to higher energies was observed for the two carbonyl IR absorption bands of the W analogue **5**$^-$ upon oxidation (**Figure S1; Table 3**).

Table 3. CO stretches observed for **3**$^-$ and **5**$^-$ under different IR-SEC cell conditions.

Cell conditions:	0.1 V	0.8 V	0.1 V	0.8 V
DPhAT added:	no	no	yes	yes
Compound:	ν_{CO}	ν_{CO}	ν_{CO}	ν_{CO}
K[MoTtz(CO)$_3$] (**3**$^-$)	1774, 1905	1894, 2021	1792, 1919	1911, 2036
Cell conditions:	**0.1 V**	**0.6 V**	**0.1 V**	**0.7 V**
Acid added[b]:	**no**	**no**	**yes**	**yes**
Compound:	ν_{CO}	ν_{CO}	ν_{CO}	ν_{CO}
K[WTtz(CO)$_3$] (**5**$^-$)	1766, 1895	1880, 2003	1791,[a] 1919[a]	1911, 2016
Assignment:	[M^{0}Ttz]$^-$	M^{1}Ttz	M^{0}HTtz	[M^{I}HTtz]$^+$

[a] Minor peaks; major peaks occur at 2022, and 1936 cm^{-1}, indicating oxidation [b] 2-methoxypyridinium triflate

Consistent with our earlier observations for the Mo-based **3**$^-$, treatment with acid in the IR-SEC cell with electrolyte resulted in monoprotonation, as evidenced by a modest shift $\Delta\nu_{CO}$ to higher frequency (**Table 1**). However, in the case of the W-based analogue **5**$^-$, data collected in the IR-SEC cell differed significantly from the salt plate data (**Table 1**). Even without a cell potential applied, as well as at 0.1 V vs NHE, the dominant IR bands at 2022 and 1936 cm^{-1} suggest that oxidation of the tungsten metal center occurred in the presence of the acid and electrolyte. An additional set of less intense (~20% of major) bathochromic absorbance bands at 1791 and 1911 cm^{-1} are fully consistent with glaze data, as well as DFT calculations for [W^0(HTtz)(CO)$_3$], **5H**. When the potential of this sample is shifted to 0.7 V (NHE), the feature at 1936 cm^{-1} diminishes in intensity, suggestive of a further oxidation process occurring. Oddly, the feature at 2022 cm^{-1} shifts only slightly, but does not decrease in intensity.

Of note, the oxidation of the Mo complex **3**$^-$ to **3** seems to result in a loss in symmetry, as signalled by the splitting of the absorbance bands seen in **Figure 6**. DFT calculations suggest that one of the M-CO bonding distances shortens upon oxidation for both Mo and W, a Jahn-Teller distortion of the low-spin octahedral d^5 complex, *vide infra*. Given that this occurs both under neutral and acidic conditions, the loss of symmetry cannot be attributed to protonation alone. For both Mo and W metal centers, the calculated $\Delta\nu_{CO}$ for protonation ranged from 9-17 cm^{-1}, similar to that observed experimentally. Regarding the metal oxidation, calculations predict a $\Delta\nu_{CO}$ of 100-134 cm^{-1}, slightly larger than our observed values.

Table 4. DFT predicted CO stretches for the protonation and one-electron oxidation products of $\mathbf{3}^-$ and $\mathbf{5}^-$.

Compound	ν_{CO}	ν_{CO}
$[Mo^0Ttz(CO)_3]^-$, $\mathbf{3}^-$	1936	1769
$[Mo^ITtz(CO)_3]$, **3**	2063	1879
$[Mo^0HTtz(CO)_3]$, **3H**	1945	1786
$[Mo^IHTtz(CO)_3]^+$, $\mathbf{3H}^+$	2073	1937
$[W^0Ttz(CO)_3]^-$, $\mathbf{5}^-$	1915	1745
$[W^ITtz(CO)_3]$, **5**	2037	1879
$[W^0HTtz(CO)_3]$, **5H**	1926	1762
$[W^IHTtz(CO)_3]^+$, $\mathbf{5H}^+$	2047	1900

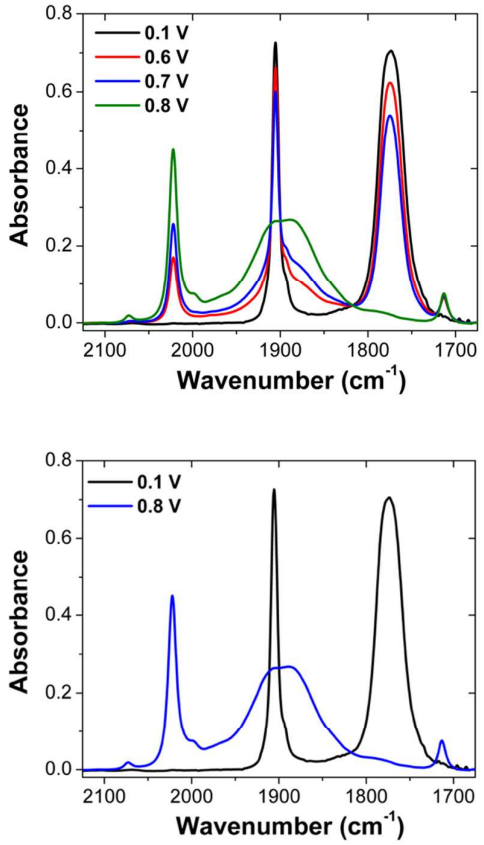

Figure 6. IR-SEC spectra of $K[MoTtz(CO)_3]$ ($\mathbf{3}^-$) (0.013 M) showing the oxidation process (top) and the spectra obtained before and after oxidation (bottom). Conditions: glassy carbon working electrode, glassy carbon counter electrode, Ag bare metal pseudo-reference electrode; internal ferrocene reference; referenced to NHE.

Given the Nernstian relationship of the oxidation potentials of $\mathbf{3}^-$ and $\mathbf{5}^-$ to the presence of different concentrations of acid, as well as the 3.5 order of magnitude shift in acid pK_a, IR-SEC was also used to monitor for possible products of proton-coupled electron transfer (PCET). This PCET reaction is mechanistically best described as proton donation from an exo-4-N atom, induced by the one-electron oxidation of the Mo^0 or W^0 metal center.

At a concentration of 0.013 M analyte and 0.04 M 2-methoxypyridinium triflate, the IR spectrum indicates that the Ttz ligand is largely monoprotonated **3H** (**Figure S5**). Upon the application of potentials capable of oxidizing the Mo center, only the deprotonated and oxidized form of the Mo^I complex **3** is observed, consistent with the half-reaction in eq 1 (**Figures 7, S4 and S5**). This result is consistent with the PCET reaction predicted by the Nernstian concentration diagrams detailed above. If a much stronger acid, DPhAT, is used, deprotonation upon oxidation does not occur (**Figure S6 and S7**), resulting in the observation of $\mathbf{3H}^+$. These cationic species exhibit a consistent shift to higher wavenumbers that is also predicted by the DFT results relative to the neutral species **3** (**Table 4**). Similar data is obtained for $\mathbf{5}^-$ under these conditions: 2-methoxypyridinium is only capable of protonating the anionic starting complex (**Figures S2, S8-S11**) with deprotonation observed upon oxidation (**Figure 7**).

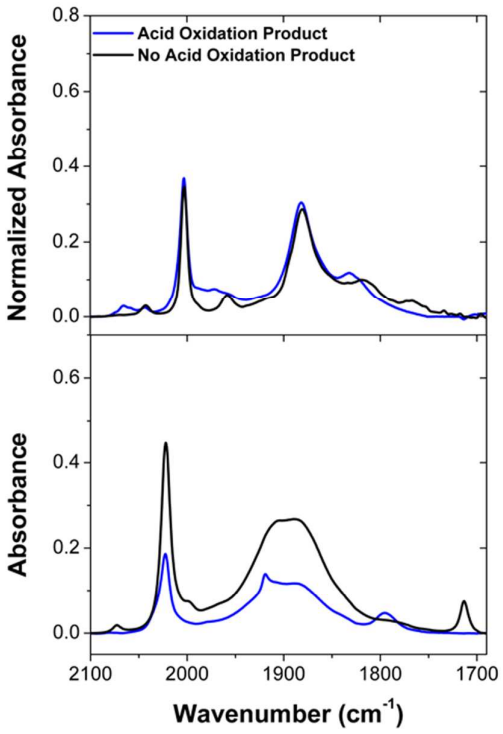

Figure 7. Infrared spectra of $[MoTtz(CO)_3]^-$ ($\mathbf{3}^-$) and $[WTtz(CO)_3]^-$ ($\mathbf{5}^-$) comparing the electrochemical oxidation products with and without addition of 2-methoxypyridinium triflate. Conditions: $\mathbf{5}^-$ (normalized): with (0.013 M analyte; 0.058 M acid) and without (0.019 M analyte). $\mathbf{3}^-$: (0.013 M) with and without added 2-methoxypyridinium triflate (0.04 M); glassy carbon working electrode, glassy carbon counter electrode, Ag bare metal pseudoreference electrode; internal ferrocene reference; referenced to NHE.

The observation of a monoprotonated product for the Mo and W congeners is in contrast to the results obtained for $Cu(Ttz^{tBu,Me})(CO)$, which reported two accessible protonations with similar pK_a^{H2O} values (~3.5).[22] The data obtained for the Cu-based system used HBF_4 in CH_2Cl_2, a superacid under these conditions,[30] with an estimated pK_a^{DCE} of -10.3. The authors

also performed the titration in an AN/H_2O mixture, where the acidity is leveled to that of aqueous H^+. Experimentally, a second protonation of a Ttz ligand is possible under those conditions, but with the weaker acids and Group VI metals used in this report, it is likely separated in pK_a from the first protonation.

DFT Results

The results from DFT calculations mentioned above were also used to provide insight into the changes in electronic structure induced by protonation and oxidation. The optimized structure of **3**$^-$ is shown in **Figure 8**; Kohn-Sham orbitals for the HOMO suggest electron density primarily on the Mo metal center and molecular orbitals involving the lone pair of the exo nitrogen atoms are not observed until HOMO-7. Consistent results are obtained for similar calculations on **5**$^-$ (**Figure S12**).

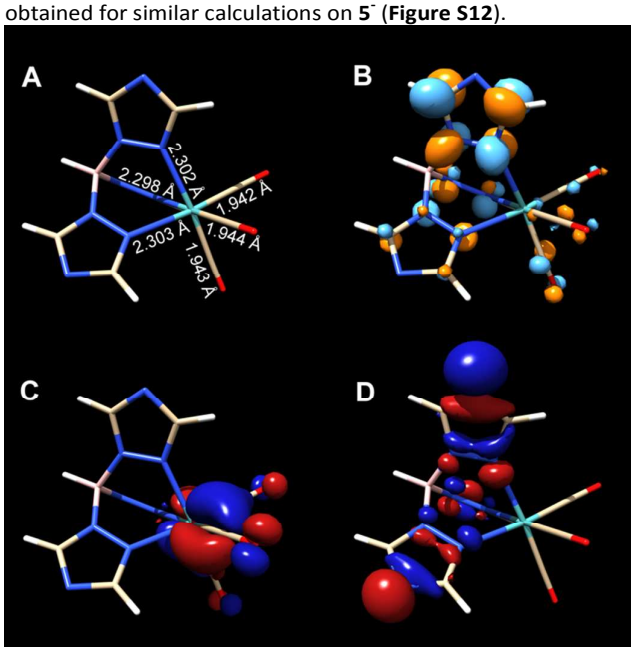

Figure 8. Kohn-Sham orbital representations of $[MoTtz(CO)_3]^-$ **3**$^-$ (A); LUMO (B); HOMO (C); and (D) HOMO-7. ORCA 4.0.0; B3LYP/G; ZORA; def2-TZVP; CPCM(Acetonitrile).

A comparison of calculated Mulliken charges between **3**$^-$ and the product of protonation **3H** suggests that a minimal change in charge on the Mo center occurs (**Table S1**). As expected, the SOMO of the oxidized **3** is almost exclusively metal-based, with corresponding increase in charge and spin population on the Mo predicted by Mulliken analysis (**Figure S13; Table S1**). The low-lying HOMO-7 orbital of **3**$^-$ is altered significantly by protonation in **3H**, as well as the LUMO, which both become predominantly localized on the protonated triazolyl ring. Minimal changes in N–Mo bond length are observed upon protonation, suggesting that the change in the interaction strength between the Ttz ligand and the metal center is relatively minor (N–Mo distance for **3**$^-$: 2.302, 2.303, and 2.298 Å; **3H** 2.305 (protonated exo N), 2.297, and 2.296 Å). The one-electron oxidation product **3**, however, shows diminished bond lengths, consistent with a stronger interaction between the now cationic metal center and the anionic Ttz ligand (N–Mo distance for **3**: 2.229, 2.232, and 2.265 Å).

The protonation product **3H** and the corresponding one-electron oxidized **3H**$^+$ show analogous changes in the electronic structure of the Mo center to those observed between **3**$^-$ and **3**, with the exception of the protonated triazolyl ring, which has miminal contribution to the HOMO-7 orbital level (**Figures S14 and S15**). Consistent with the experimental data described above, similar trends are observed for **5**$^-$ (**Figures S16-S18**). These results suggest that the protonation-induced redox behavior of the framework is largely the result of an electrostatic effect; the primary bonding interactions between the ligand and metal center are predicted to remain intact at this level of theory. Consistent with the splitting of the low frequency absorbance bands observed by IR for the oxidized species, the DFT calculations show the effects of Jahn-Teller distortion: one of the three M-CO bonds in **3**, **3H**$^+$, **5**, and **5H**$^+$ decreases relative to the others (see **Figures S13, S15, S16, and S18**).

Lewis Acid-Induced Redox Modulation

Having demonstrated a reversible Brønsted acid-induced modulation of the redox behavior for the Ttz complexes **3**$^-$ and **5**$^-$, we were interested in exploring the generality of these observations with respect to Lewis acids. As a proof of concept, we initially explored the use of trifluoroborane etherate (BF_3•Et_2O) as a Lewis acid additive. When one molar equivalent (0.01 M) of BF_3•Et_2O was added to **3**$^-$ or **5**$^-$, a new redox feature began to develop in the voltammogram, with an $E_{1/2}$ ~200 mV positive of the original feature. This feature continued to grow proportionally with concomitant loss of the redox wave corresponding to the starting material as more BF_3•Et_2O was added. Once 5 molar equivalents of the BF_3•Et_2O had been added (final concentration 0.05 M), the voltammogram showed only the new redox couple (**Table 2; Figures S19 and S20**). IR data for the purported [**3**]•BF_3 show peaks at 1787 and 1920 cm^{-1}, while [**5**$^-$]•BF_3 IR data show absorbance bands at 1788 and 1911 cm^{-1}, a similar shift to that observed with Brønsted acids.

In the case of Mo, the use of BF_3•Et_2O at low concentrations produces changes in the ^{1}H NMR spectrum consistent with the formation of a monoadduct. The addition of 1 equivalent of BF_3•Et_2O to **3**$^-$ produced distinct new triazolyl signals, appearing in a 2:1 ratio, reminiscent of the monoprotonated product described above. Higher concentrations (up to 0.1 M; 10 eq) of the Lewis acid generated multiple sets of proton resonances, but no species consistent with triadduct formation was observed (**Figure S22)**, suggesting that BF_3•Et_2O is only capable of generating a diadduct under these conditions.

Conclusions

The use of exogenous acids to tune redox behavior *via* chemical interactions with the exo N atoms of the Ttz ligand framework was explored using the tricarbonyl species $[Mo(Ttz)(CO)_3]^-$ **3**$^-$ and $[W(Ttz)(CO)_3]^-$ **5**$^-$ as model compounds.

When the weak Brønsted acids pyridinium triflate and (p-methoxyanilinium)[BF_4] were added to a solution of $\mathbf{3}^-$ and $\mathbf{5}^-$, shifts in the observed ^{1}H NMR resonances consistent with monoprotonation were observed. Equilibration with these acids under these conditions also enabled the determination of the pK_a values for **3H** and **5H**.

Examination of this monoprotonation reaction by electrochemical techniques revealed that the M(I)/(0) redox feature shifted to positive potentials by ~200 mV. Notably, the electrochemical response showed a Nernstian proton donor to electron ratio when $E_{1/2}$ was plotted against $\log_{10}([A]/[HA^+])$, consistent with a PCET reaction upon one electron oxidation of the parent species **3H** and **5H**. These data were used to construct a thermochemical cycle that determined the pK_a $\mathbf{3H}^+$ and $\mathbf{5H}^+$ to be lower than **3H** and **5H** by 3.5.

These assignments were verified using IR-SEC, which confirmed changes in protonation upon oxidation. Further, the use of DPhAT and triflic acid (which have much lower pK_a values than (2-methoxypyridinium)[BF_4] and (p-methoxyanilinium)[BF_4]), showed that these compounds can remain protonated upon oxidation in the presence of a suitable acid. Preliminary studies with the Lewis acid BF_3 suggest that this behavior at the exo-4-N atom may be generalizable with respect to other additives, studies exploring this are currently underway.

Experimental Section

General Methods. NMR spectra were obtained on 600 or 800 MHz spectrometers. Chemical shifts are referenced to tetramethylsilane (TMS) utilizing residual ^{1}H signals of the deuterated solvents as internal standards. Chemical shifts are reported in ppm and coupling constants (J) are reported in hertz (Hz). Infrared Spectra (IR) were recorded on a spectrometer as a glaze on a Horizontal Attenuated Total Reflectance (HATR) accessory, or as a glaze between two NaCl plates, with peaks reported in cm^{-1}. Electrochemical experiments were performed under a nitrogen atmosphere. Cyclic voltammetric data were recorded at ambient temperature at 100 mV/s unless otherwise noted, with a standard three electrode cell from +1.8 V to -1.8 V with a platinum working electrode, *N,N*-dimethylacetamide (DMA) or acetonitrile (MeCN) solvent, and tetrabutylammonium hexafluorophosphate (TBAH) electrolyte (~1.0 M). For CV data recorded in aqueous solutions, sodium triflate (NaOTf) was used as the electrolyte. All potentials are reported versus the normal hydrogen electrode (NHE) using cobaltocenium hexafluorophosphate ($E_{1/2}$ = -0.78 V, -1.75 V) or ferrocene ($E_{1/2}$ = 0.55 V) as an internal standard. Peak separation of all reversible couples was less than 100 mV. All synthetic reactions were performed in a glovebox under a dry nitrogen atmosphere unless otherwise noted. All solvents were purged with nitrogen prior to use. Deuterated solvents were used as received from Cambridge Isotopes. Compounds $\mathbf{2}^-$, $\mathbf{4}^-$, **6**, and **8** were prepared according to previous literature methods,[5,26] and characterization of **1**, $\mathbf{3}^-$, and **7** by ^{1}H and ^{13}C NMR, as well as CV and IR, is consistent with the findings reported by Shiu and co-workers.[11]

K[Ttz] (potassium hydrotris(1,2,4-triazol-1-yl)borate) (1) A mixture of 1,2,4-triazole (250 g, 3.62 mol) and KBH_4 (43.4g, 0.804 mol) was added to a 1 L round bottom flask and placed in an oil bath preheated to 125 °C. The flask was fitted with a N_2 line and a cold-finger condenser containing dry-ice/acetone. The 1,2,4-triazole melted over 10 min and dissolved the KBH_4, giving a colorless molten solution and H_2 evolution (CAUTION!). The oil bath temperature was then slowly increased to 200 °C over the course of 15 min, with continuous H_2 evolution. The molten solution was allowed to stir at 200 °C for 2 h. The N_2 line was then removed and the excess 1,2,4-triazole was removed in vacuo for 20 min, until the molten solution became a white solid, and triazole began to deposit on the cold finger. The reaction mixture was then removed from the oil bath and allowed to cool to room temperature. The resulting solid was washed with acetone (4 x 200 mL) and desiccated giving (**1**) (168.17 g, 82%).

K[MoTtz(CO)$_3$] (potassium tricarbonyl(hydrotris(1,2,4-triazol-1-yl)borate)molybdenum(0)) ($\mathbf{3}^-$) Compound **1** (69.58 g, 0.237 mol), $Mo(CO)_6$ (68.98 g, 0.261 mol), and MeOH (700 mL) were added to a 2 L round bottom flask charged with a stir bar, giving a yellow mixture. The flask was fitted with a reflux condenser and was placed in a heating mantle. The reaction mixture was refluxed overnight (16 h), giving a bright yellow mixture, which was removed from heat and cooled to room temperature. The mixture was filtered through a 600 mL fine frit, and the filtercake was washed with MeOH (2 x 250 mL) followed by Et_2O (3 x 250 mL). The yellow solid (**3**) was collected and desiccated (87%, 89.71 g, 0.206 mol).

K[WTtz(CO)$_3$] (potassium tricarbonyl(hydrotris(1,2,4-triazol-1-yl)borate)tungsten(0)) ($\mathbf{5}^-$) Compound **1** (38.61 g, 0.151 mol), $W(CO)_6$ (51.85 g, 0.147 mol), and diglyme (250 mL) were added to a 1 L round bottom flask charged with a stir bar, giving a yellow mixture. The flask was fitted with a reflux condenser and was placed in a heating mantle. The reaction mixture was refluxed overnight (16 h), giving a bright yellow mixture, which was removed from heat and cooled to room temperature. The mixture was filtered through a 350 mL fine frit and the filtercake was washed with MeOH (2 x 150 mL) followed by Et_2O (3 x 150 mL) and the product (**5**) was desiccated and collected. (88%, 67.65 g, 0.129 mol). ^{1}H NMR (DMSO-d_6, δ): 8.15 (s, 3H); 8.61 (s, 3H). ^{13}C NMR (DMSO-d_6, δ): 148.5, 154.5. CV: $E_{1/2}$ = -0.07 V. IR: ν_{CO} = 1684, 1856 cm^{-1}; ν_{BH} = 2481 cm^{-1}. Reactivity of $\mathbf{5}^-$ with air prevented a satisfactory CHN analysis.

MoTtz(NO)(CO)$_2$ (dicarbonylnitrosyl(hydrotris(1,2,4-triazol-1-yl)borate)molybdenum(0)) (7) Compound **1** (50.17 g, 0.197 mol), $Mo(CO)_6$ (49.93 g, 0.189 mol), and MeOH (500 mL) were added to a 1 L round bottom flask charged with a stir bar, giving a yellow mixture. The flask was fitted with a reflux condenser and was placed in a heating mantle. The reaction mixture was refluxed overnight (14 h), giving a bright yellow mixture, which was removed from heat and cooled to room temperature. The mixture was then

poured into a 1 L Erlenmeyer flask, in an ice bath, and charged with $NaNO_2$ (14.51 g, 0.210 mol) and a stir bar. Acetic acid (50 mL, 0.874 mol) was added to the stirring solution, giving a color change to orange and the evolution of gas. After stirring for 30 min, the mixture was filtered through a 600 mL medium frit, and the product (**7**) was washed with H_2O (5 x 400 mL) followed by Et_2O (3 x 400 mL) and then desiccated. (83%, 62.75 g, 0.158 mol). ^{1}H NMR (DMSO-d_6, δ): 8.90 (s, 2H); 8.75 (s, 2H); 8.85 (s, 1H); 8.73 (s, 1H). ^{13}C NMR (DMSO-d_6, δ): 150.5, 150.6, 156.1, 156.3. CV: $E_{p,a}$ = +1.30 V. IR: ν_{NO} = 1654 cm^{-1} ν_{CO} = 1910, 2010 cm^{-1}; ν_{BH} = 2533 cm^{-1}. Anal. Calcd for $C_8H_7BN_{10}O_3Mo$: C, 24.14; H, 1.77; N, 35.2 Found: C, 24.42; H, 1.57; N, 35.22.

WTtz(NO)(CO)2 (9) Compound **1** (44.37 g, 0.174 mol), $W(CO)_6$ (58.77 g, 0.167 mol), and DMF (500 mL) were added to a 1 L round bottom flask charged with a stir bar, giving a yellow mixture. The flask was fitted with a reflux condenser and was placed in a heating mantle. The reaction mixture was refluxed overnight (16 h), giving a bright yellow mixture, which was removed from heat and cooled to room temperature. The mixture was then poured into a 2 L Erlenmeyer flask, charged with $NaNO_2$ (12.11 g, 0.176 mol) and a stir bar, and placed in an ice bath. Acetic acid (50 mL, 0.847 mol) was added to the stirring solution, giving a color change to orange and evolution of gas. After stirring for 30 min, the mixture was filtered through a 600 mL medium frit, and the filtercake was washed with H_2O (5 X 400 mL) followed by Et_2O (3 X 400 mL). The orange solid was desiccated giving (**9**) (79%, 68.99 g, 0.1342 mol). ^{1}H NMR (DMSO-d_6, δ): 8.80 (s, 1H); 8.84 (s, 2H); 8.90 (s, 1H); 8.95 (s, 2H). ^{13}C NMR (DMSO-d_6, δ): 150.1, 150.1, 156.1, 156.4. CV: $E_{p,a}$ = +1.26 V. IR: ν_{NO} = 1636 cm^{-1} ν_{CO} = 1884, 1994 cm^{-1}; ν_{BH} = 2550 cm^{-1}. Anal. Calcd for $C_8H_7BN_{10}O_3W$: C, 19.78; H, 1.45; N, 28.83 Found: C, 19.89; H, 1.25; N, 28.67.

Infrared Spectroelectrochemistry. All IR-SEC experiments were conducted using a custom cell based on a previously published design.[34,36] A Bruker Vertex V80 with LN_2-cooled detector was used to collect all spectra. The three-electrode set-up consists of an inner glassy carbon working electrode disc (10 mm diameter), a central circular silver bare metal pseudoreference electrode, and an outer circular glassy carbon counter electrode embedded within a PEEK block. All data were referenced to an internal ferrocene standard (ferrocinium/ferrocene reduction potential under stated conditions); obtained by taking a CV with a blank solution in the cell prior to injecting analyte for IR-SEC experiments) unless otherwise specified. All spectra were processed by subtraction of a data obtained without analyte present at resting potential.

Computational Methods. DFT calculations were performed on the Rivanna High-Performance Computing Cluster at the University of Virginia using ORCA 4.0.0.[37] Geometry optimizations were performed unrestricted with the B3LYP/G[38-42] functional and ZORA-def2-TZVP[43] basis set (def2/J[44] and SARC/J[45-47]auxiliary basis sets where necessary) with the RIJCOSX approximation, D3BJ dispersion correction[48,49], and CPCM[50] to model the AN solvent. Numerical frequency calculations at the same level of theory were performed to validate the optimized geometries as minima on the potential energy surface and to generate thermochemical data.

Conflicts of interest

There are no conflicts to declare.

Acknowledgements

The authors gratefully acknowledge the National Science Foundation (CHE-1152803) and ARCS for support with the Rivanna High-Performance Computational Cluster.

References

1 Trofimenko, S. Boron-Pyrazole Chemistry. *J. Am. Chem. Soc.* 1966, *88*, 1842-1844.
2 Trofimenko, S. Scorpionates: Polypyrazolylborate Ligands and Their Coordination Chemistry. Imperial College Press, 1999.
3 Trofimenko, S. Boron-pyrazole chemistry. II. Poly(1-pyrazolyl)-borates. *J. Am. Chem. Soc.* 1967, *89*, 3170-3177.
4 Trofimenko, S. Scorpionates: genesis, milestones, prognosis. *Polyhedron* 2004, *23*, 197-203.
5 Trofimenko, S. Transition metal polypyrazolylborates containing other ligands. *J. Am. Chem. Soc.* 1969, *91*, 588-595.
6 Trofimenko, S. Geminal poly(1-pyrazolyl)alkanes and their coordination chemistry. *J. Am. Chem. Soc.* 1970, *92*, 5118-5126.
7 Ritter, S. K. Pinch and Sting: the Scorpionates. *Chem. Eng. News* 2003, *81*, 40-43.
8 Lobbia, G. G.; Bonati, F.; Ceccih, P. A Preparation of Potassium Tris(1,2,4-Triazol-1-yl)hydroborate and of Some Metal Derivatives. *Synth. React. Inorg. Met.-Org. Chem.* 1991, *21*, 1141-1151.
9 (9) Effendy; Gioia Lobbia, G.; Marchetti, F.; Pellei, M.; Pettinari, C.; Pettinari, R.; Santini, C.; Skelton, B. W.; White, A. H. Syntheses and spectroscopic and structural characterization of silver(I) complexes containing tris(isobutyl)phosphine and poly(azol-1-yl)borates. *Inorg. Chim. Acta* 2004, *357*, 4247-4256.
10 Lobbia, G. G.; Pellei, M.; Pettinari, C.; Santini, C.; Skelton, B. W.; White, A. H. Silver (I) poly(1,2,4-triazolyl)borate complexes containing monodentate phosphane ligands. *Inorg. Chim. Acta* 2005, *358*, 1162-1170.
11 Shiu, K.-B.; Lee, J. Y.; Yu, W.; Ming-Chu, C.; Sue-Lein, W.; Fen-Ling, L. Structures and properties of molybdenum carbonyl complexes containing uninegative nitrogen-tripod ligands derived from heterocyclic compounds including 1-H-pyrazole and 1-H-1,2,4-triazole. *J. Organomet. Chem.* 1993, *453*, 211-219.
12 Shiu, K.-B.; Guo, W.-N.; Peng, S.-M.; Cheng, M.-C. Synthesis, Structure, Reactivity, and Solution Behavior of Bis{dicarbonyl[hydridotris(1,2,4-triazolyl)borato]ruthenium(I)}(Ru-Ru). *Inorg. Chem.* 1994, *33*, 3010-3013.
13 Tang, H.; Lu, D. Multiple-Site SO2-Capture Ionic Liquids with Nearly Uniform Site Performance. *Chem., Phys. Chem. Anwendungstech. Grenzflaechenakt. Stoffe, Ber. Int. Kongr., 6th* 2015, *16*, 2854-2860.
14 Youm, K.-T.; Kim, M. G.; Ko, J.; Jun, M.-J. A Noninterpenetrating Three-Dimensional 4669 Iron(ii)

Coordination Polymer Built with a Trigonal-Antiprismatic Iron(iii) Metalloligand. *Angew. Chem., Int. Ed.* 2006, *45*, 4003-4007.
15 Bongiovanni, J. L.; Rowe, B. W.; Fadden, P. T.; Taylor, M. T.; Wells, K. R.; Kumar, M.; Papish, E. T.; Yap, G. P. A.; Zeller, M. Synthesis, structural studies and solubility properties of zinc(II), nickel(II) and copper(II) complexes of bulky tris(triazolyl)borate ligands. *Inorg. Chim. Acta* 2010, *363*, 2163-2170.
16 Gardner, S. R.; Papish, E. T.; Monillas, W. H.; Yap, G. P. A. Tris(triazolyl)borate ligands of intermediate steric bulk for the synthesis of biomimetic structures with hydrogen bonding and solubility in hydrophilic solvents. *Journal of Inorganic Biochemistry* 2008, *102*, 2179-2183.
17 Jernigan, F. E.; Sieracki, N. A.; Taylor, M. T.; Jenkins, A. S.; Engel, S. E.; Rowe, B. W.; Jové, F. A.; Yap, G. P. A.; Papish, E. T.; Ferrence, G. M. Sterically Bulky Tris(triazolyl)borate Ligands as Water-Soluble Analogues of Tris(pyrazolyl)borate. *Inorg. Chem.* 2007, *46*, 360-362.
18 Kumar, M.; Papish, E. T.; Zeller, M.; Hunter, A. D. Zinc complexes of TtzR,Me with O and S donors reveal differences between Tp and Ttz ligands: acid stability and binding to H or an additional metal (TtzR,Me = tris(3-R-5-methyl-1,2,4-triazolyl)borate; R = Ph, tBu). *Dalton Trans.* 2011, *40*, 7517-7533.
19 Kumar, M.; DePasquale, J.; White, N. J.; Zeller, M.; Papish, E. T. Ruthenium Complexes of Triazole-Based Scorpionate Ligands Transfer Hydrogen to Substrates under Base-Free Conditions. *Organometallics* 2013, *32*, 2135-2144.
20 Macleod, I. T.; Tieknik, E. R. T.; Young, C. G. Carbonyl-molybdenum complexes of the hydrotris(3,5-dimethyl-1,2,4-triazol-1-yl) borate ligand. *J. Organomet. Chem.* 1996, *506*, 301-306.
21 Papish, E. T.; Donahue, T. M.; Wells, K. R.; Yap, G. P. A. How are tris(triazolyl)borate ligands electronically different from tris(pyrazolyl)borate ligands? A study of (TttztBu,Me)CuCO [TttztBu,Me = tris(3-t-butyl-5-methyl-1,2,4-triazolyl)borate]. *Dalton Trans.* 2008, 2923-2925.
22 Dixon, N. A.; McQuarters, A. B.; Kraus, J. S.; Soffer, J. B.; Lehnert, N.; Schweitzer-Stenner, R.; Papish, E. T. Dramatic tuning of ligand donor properties in (Ttz)CuCO through remote binding of H+ (Ttz = hydrotris(triazolyl)borate). *Chem. Commun.* 2013, *49*, 5571-5573.
23 Oseback, S. N.; Shim, S. W.; Kumar, M.; Greer, S. M.; Gardner, S. R.; Lemar, K. M.; DeGregory, P. R.; Papish, E. T.; Tierney, D. L.; Zeller, M.; Yap, G. P. A. Crowded bis ligand complexes of TtzPh,Me with first row transition metals rearrange due to ligand field effects: structural and electronic characterization (TtzPh,Me = tris(3-phenyl-5-methyl-1,2,4-triazolyl)borate). *J. C. S., Dalton Trans.* 2012, *41*, 2774-2787.
24 Gunnoe, T. B.; Sabat, M.; Harman, W. D. Reactions of TpRe(CO)2(THF) with Aromatic Molecules (Tp = Hydridotris(pyrazolyl)borate). *J. Am. Chem. Soc.* 1998, *120*, 8747-8754.
25 Liebov, B. K.; Harman, W. D. Group 6 Dihapto-Coordinate Dearomatization Agents for Organic Synthesis. *Chem. Rev.* 2017.
26 McCleverty, J. A.; Seddon, D.; Bailey, N. A.; Walker, N. W. The chemistry of cyclopentadienyl and related nitrosyl complexes of molybdenum. Part V. Dihalogenonitrosyl[tris(pyrazolyl)borato]molybdenum complexes, their alcoholysis, and the crystal structure of chloronitrosylisopropoxo[tris(4-chloro-3,5-dimethylpyrazolyl)borato]molybdenum. *J. C. S., Dalton Trans.* 1976, 898-908.
27 Dilsky, S.; Palomaki, P. K. B.; Rubin, J. A.; Saunders, J. E.; Pike, R. D.; Sabat, M.; Keane, J. M.; Ha, Y. Synthesis and reactivity of cationic bipyridine tungsten(0) and molybdenum(0) nitrosyl complexes. *Inorg. Chim. Acta* 2007, *360*, 2387-2396.
28 Lu, D.; Tang, H. Theoretical survey of the ligand tunability of poly(azolyl)borates. *Phys. Chem. Chem. Phys.* 2015, *17*, 17027-17033.
29 Eckert, F.; Leito, I.; Kaljurand, I.; Kütt, A.; Klamt, A.; Diedenhofen, M. Prediction of acidity in acetonitrile solution with COSMO-RS. *J. Comput. Chem.* 2009, *30*, 799-810.
30 Kütt, A.; Rodima, T.; Saame, J.; Raamat, E.; Mäemets, V.; Kaljurand, I.; Koppel, I. A.; Garlyauskayte, R. Y.; Yagupolskii, Y. L.; Yagupolskii, L. M.; Bernhardt, E.; Willner, H.; Leito, I. Equilibrium Acidities of Superacids. *The J. Org. Chem.*2011, *76*, 391-395.
31 Kilgore, U. J.; Roberts, J. A. S.; Pool, D. H.; Appel, A. M.; Stewart, M. P.; DuBois, M. R.; Dougherty, W. G.; Kassel, W. S.; Bullock, R. M.; DuBois, D. L. [Ni(PPh2NC6H4X2)2]2+ Complexes as Electrocatalysts for H2 Production: Effect of Substituents, Acids, and Water on Catalytic Rates. *J. Am. Chem. Soc.* 2011, *133*, 5861-5872.
32 Bordwell, F. G. Equilibrium acidities in dimethyl sulfoxide solution. *Acc. Chem. Res.* 1988, *21*, 456-463.
33 Kaljurand, I.; Kutt, A.; Soovali, L.; Rodima, T.; Maemets, V.; Leito, I.; Koppel, I. Extension of the Self-Consistent Spectrophotometric Basicity Scale in Acetonitrile to a Full Span of 28 pK_a Units: Unification of Different Basicity Scales. *J. Org. Chem.*2005, *70*, 1019-1028.
34 McCarthy, B. D.; Dempsey, J. L., Decoding Proton-Coupled Electron Transfer with Potential–pKa Diagrams. Inorg. Chem. 2017, 56, 1225-1231.
35 Machan, C.; Sampson, M.; Chabolla, S.; Dang, T.; Kubiak, C. Developing a Mechanistic Understanding of Molecular Electrocatalysts for CO2 Reduction using Infrared Spectroelectrochemistry. *Organometallics* 2014, *33*, 4550-4559.
36 Zavarine, I. S.; Kubiak, C. P. A versatile variable temperature thin layer reflectance spectroelectrochemical cell. *J. Electroanal. Chem.* 2001, *495*, 106-109.
37 Neese, F. The ORCA program system. *Wiley Interdisciplinary Reviews: Computational Molecular Science* 2012, *2*, 73-78.
38 Vosko, S. H.; Wilk, L.; Nusair, M. Accurate spin-dependent electron liquid correlation energies for local spin density calculations: a critical analysis. *Can. J. Phys.* 1980, *58*, 1200-1211.
39 Lee, C.; Yang, W.; Parr, R. G. Development of the Colle-Salvetti correlation-energy formula into a functional of the electron density. *Phys. Rev. B* 1988, *37*, 785-789.
40 Becke, A. D. Density-functional thermochemistry. III. The role of exact exchange. *J. Chem. Phys.* 1993, *98*, 5648-5652.
41 Becke, A. D. A new mixing of Hartree–Fock and local density-functional theories. *J. Chem. Phys.* 1993, *98*, 1372-1377.
42 Stephens, P. J.; Devlin, F. J.; Chabalowski, C. F.; Frisch, M. J. Ab Initio Calculation of Vibrational Absorption and Circular Dichroism Spectra Using Density Functional Force Fields. *J. Phys. Chem.* 1994, *98*, 11623-11627.
43 Izsák, R.; Neese, F. An overlap fitted chain of spheres exchange method. *J. Chem. Phys.* 2011, *135*, 144105.
44 Weigend, F. Accurate Coulomb-fitting basis sets for H to Rn. *Phys. Chem. Chem. Phys.* 2006, *8*, 1057-1065.
45 Pantazis, D. A.; Neese, F. All-Electron Scalar Relativistic Basis Sets for the Lanthanides. *J. Chem. Theory Comput.* 2009, *5*, 2229-2238.
46 Pantazis, D. A.; Chen, X.-Y.; Landis, C. R.; Neese, F. All-Electron Scalar Relativistic Basis Sets for Third-Row Transition Metal Atoms. *J. Chem. Theory Comput.* 2008, *4*, 908-919.
47 Pantazis, D. A.; Neese, F. All-electron scalar relativistic basis sets for the 6p elements. *Theor. Chem. Acc.* 2012, *131*, 1292.

48 Grimme, S.; Antony, J.; Ehrlich, S.; Krieg, H. A consistent and accurate ab initio parametrization of density functional dispersion correction (DFT-D) for the 94 elements H-Pu. *J. Chem. Phys.* 2010, *132*, 154104.
49 Grimme, S.; Ehrlich, S.; Goerigk, L. Effect of the damping function in dispersion corrected density functional theory. *J. Comput. Chem.* 2011, *32*, 1456-1465.
50 Cossi, M.; Rega, N.; Scalmani, G.; Barone, V. Energies, structures, and electronic properties of molecules in solution with the C-PCM solvation model. *J. Comput. Chem.* 2003, *24*, 669-681.
51 Koelle, U.; Infelta, P. P.; Grätzel, M., Kinetics and Mechanism of the Reduction of Protons to Hydrogen by Cobaltocene. Inorganic Chemistry 1988, 27, 879-883.

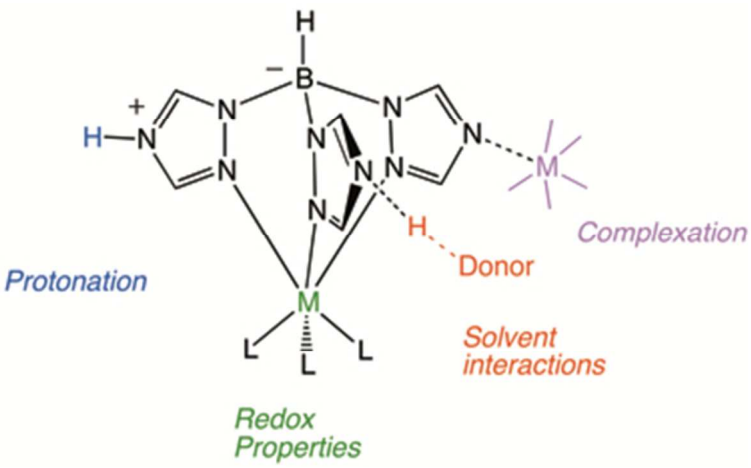

132x81mm (72 x 72 DPI)